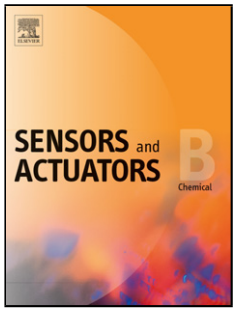

Title: Nanoporous Nb_2O_5 hydrogen gas sensor

Authors: Rozina Abdul Rani Ahmad Sabirin Zoolfakar Jian Zhen Ou Matthew R. Field Michael Austin Kourosh Kalantar-zadeh

PII: S0925-4005(12)00940-9
DOI: doi:10.1016/j.snb.2012.09.028
Reference: SNB 14550

To appear in: *Sensors and Actuators B*

Received date: 29-6-2012
Revised date: 27-8-2012
Accepted date: 11-9-2012

Please cite this article as: R.A. Rani, A.S. Zoolfakar, J.Z. Ou, M.R. Field, M. Austin, K. Kalantar-zadeh, Nanoporous Nb_2O_5 hydrogen gas sensor, *Sensors and Actuators B: Chemical* (2010), doi:10.1016/j.snb.2012.09.028

Nanoporous Nb_2O_5 hydrogen gas sensor

Rozina Abdul Rani*[,a], Ahmad Sabirin Zoolfakar[a,c], Jian Zhen Ou[a], Matthew R. Field[b], Michael Austin[a], and Kourosh Kalantar-zadeh*[,a]

[a] School of Electrical and Computer Engineering, RMIT University, Melbourne, Victoria 3001, Australia

[b] School of Applied Sciences, Applied Physics, RMIT University, Melbourne, Victoria 3001, Australia

[c] Faculty of Electrical Engineering, Universiti Teknologi MARA, 40450 Shah Alam, Malaysia

* Corresponding author: Ms. Rozina Abdul Rani and A/Prof. Kourosh Kalantar-zadeh

Mailing Address: School of Electrical and Computer Engineering, RMIT University, Melbourne, Victoria 3001, Australia

Emails: rozina.abdulrani@student.rmit.edu.au and kourosh.kalantar@rmit.edu.au

Phone: +61-3-99253254

Fax: +61-3-99253242

Abstract: This work presents the development of gas sensors based on nanoporous niobium oxide (Nb_2O_5) films for hydrogen gas sensing. Nanoporous Nb_2O_5 films were successfully synthesized by the anodization of niobium foil in fluoride-organic solvent containing a small percentage of water at 50 °C. These conditions helped to obtain nanovein-like networks with pore diameters of 30 ~ 50 nm. After annealing at 440 !C an orthorhombic phase of Nb_2O_5 was obtained. Contacts of the sensors were then established using platinum (Pt) that also acted as catalytic layers. The gas sensing properties of these nanoporous contacts were investigated for hydrogen gas sensing at different film thicknesses and temperatures.

Keywords: Niobium oxide (Nb_2O_5); Anodization; Nanoporous; Gas sensor; Hydrogen (H_2)

1. Introduction

The employment of metal oxides in gas sensing applications has been widely investigated for their capability to sense numerous types of gas species. In the past two decades, a tremendous improvement has been demonstrated in the performance of metal oxide based gas sensors *via* the transformation of the first generation thick film devices to ones incorporating nanostructured metal oxide films [1, 2]. Such nanostructured metal oxides allow the target gases to penetrate into and have access to the entire volume of the films. This maximizes the interaction of the exposed surface of the nanostructured films with the gas species and results in large changes in their physical and chemical properties [3, 4].

There are many reports on the gas sensing properties of nanostructured metal oxides such as SnO_2, ZnO, TiO_2, WO_3, In_2O_3, CuO, NiO, Ga_2O_3, and V_2O_5 [5-14]. However, a much smaller number of papers address the feasibility of Nb_2O_5 for gas sensing [15-24]. Nb_2O_5 is known as a wide band-gap *n*-type metal oxide and has desirable properties such as good chemical stability, low film stress, and a high refractive index (n = 2.4 at 550 nm) [25]. Nb_2O_5 has many different crystal phases, but the most commons are pseudo-hexagonal, orthorhombic, tetragonal and monoclinic [26]. Due to the remarkable properties of Nb_2O_5, it has been used in a variety of applications such as in catalysis and as a biocompatible material [27], in electrochromic coatings [28, 29], batteries [30], and solar cells [31, 32].

The first report on Nb_2O_5 gas sensors dates back to the early 1980s [15]. However, comprehensive reports on Nb_2O_5 mostly belong to the mid to late 1990s [16-19]. In these works, techniques such as radio frequency magnetron sputtering were used for the deposition of dense Nb_2O_5 films and operating temperatures as high as 500 ºC were implemented to sense gases such as O_2, NH_3 and CO. Porous Nb_2O_5 films for gas sensing were later reported. The first example is the work of Hyodo *et al.* who successfully developed a gas sensor based on anodic micro porous Nb_2O_5 synthesized in aqueous acidic electrolytes [20].

The interest in Nb_2O_5 has increased in the past five years with the introduction of nanostructured Nb_2O_5. Cvelbar *et al.* introduced an oxygen gas sensor based on a Nb_2O_5 nanowire array [21]. Also, Nb_2O_5 nanowires have been employed as a Schottky based hydrogen (H_2) gas sensor [24]. In this work, Nb_2O_5 nanowires were synthesized *via* a thermal oxidation process, showing repeatable responses for H_2 sensing at room temperature. To obtain nanostructured Nb_2O_5, several synthesis methods have been reported, including anodization [31, 33], sol-gel dip-coating [34], hydrothermal [35, 36], pulsed laser deposition [37], and electrodeposition [38]. Among them, the anodization method has several advantages over the others due to its low fabrication cost and controllable film thickness. It also offers the benefit of producing porous films with high aspect ratios, which is the key factor to exhibit an excellent gas sensing performance. Despite the obvious advantages of nanoporous Nb_2O_5 there is still no report on the implementation of such a structure for gas sensing applications.

Here, we introduce a gas sensor based on a novel nanoporous Nb_2O_5 film synthesized *via* an anodization process at elevated temperatures in fluoride-organic solvent containing a small amount of water content. Based on our previous studies [31], we controlled the synthesis process and produced ~1 and ~2 μm thickness of nanoporous Nb_2O_5 films for gas sensing. In this study, the devices were coated with Pt and exposed to H_2 gas of different concentrations and temperatures (in a range from room temperature to 100 °C) and their behaviors and sensing performance were investigated.

2. Experimental

2.1 Fabrication of nanoporous Nb_2O_5

Niobium foil (99.9% purity, Sigma Aldrich) of 0.25 mm thickness was cut into pieces of 1.0 cm × 1.5 cm. These niobium substrates were cleaned with acetone in an ultrasonic bath

for 5 minutes, washed with isopropanol and deionized water then dried in a stream of nitrogen gas. The electrolytes for the anodization consisted of 50 ml ethylene glycol (98% anhydrous, Sigma Aldrich), 4 vol % deionized water and 0.25 g NH_4F (98% purity, Sigma Aldrich). Details on the optimization of the anodization process is discussed in the previous work [31].

Anodization was performed using a two-electrode system consisting of an anode (niobium foil sample) and cathode (Pt), where a DC voltage of 10 V was applied while the electrolyte temperature was kept constant at 50 °C. Nanoporous Nb_2O_5 with a thickness of ~1 and ~2 μm were obtained after 0.5 and 1.0 hours of anodization, respectively. After the anodization process, the samples were washed with deionized water and dried in a nitrogen stream. Then, the samples were annealed in air at a temperature of 440 °C for 30 minutes with a slow ramp up and down rate of 2 °C/min. The as-anodized porous structure is amorphous for annealing temperatures below 440 °C, while above this temperature, the nanoporous Nb_2O_5 layer appears to be slightly cracked, possibly due to the thermal expansion effect during the oxidation (Figure S1 in the supporting information).

2.2 Structural characterization

The morphology and structural properties of the films were characterized using a FEI Nova NanoSEM scanning electron microscopy (SEM). The crystallinity of the Nb_2O_5 was characterized by a D8 Advance Bruker AXS Xray diffractor with GADDS (General Area Detector Diffraction System) attachment fitted with a 50 μm spot size collimator, incorporating a High Star 2 dimensional detector and CuKα radiation (λ = 0.1542 nm) operating at 40 kV and 40 mA. Meanwhile, the chemical compositions of the Nb_2O_5 were conducted using Thermo K-alpha X-ray Photoelectron Spectrometer (XPS). For Raman measurements, the characterizations were performed using a system incorporating an Ocean

Optic QE 6500 spectrometer, a 532 nm 40 mW laser as the excitation source and a notch filter used in order to prevent measurement below 100 cm^{-1}. To identify the distribution of Pt element in the nanoporous Nb_2O_5 films, EDAX Si(Li)X-ray detector fitted with the FEI Nova NanoSEM system was used.

2.3 Gas sensors fabrication

A Pt layer with thickness of 10 nm was deposited on both sides of the bare metal and the surface of the nanoporous Nb_2O_5 as demonstrated schematically in the cross-sectional view in Figure 1(a). One side of the bare metal layer was the extended electrode connected to the Pt layer on the surface of nanoporous Nb_2O_5. This was to avoid damage on the nanoporous structure during probing of the device. Meanwhile, photoresist was used as an insulation layer to prevent a short circuit between the extended electrode and the niobium foil. The overall configuration of the complete device is shown in Figure 1(b).

2.4 Gas sensors characterizations

All H_2 gas sensing experiments were performed in a LINKAM customized gas testing chamber. The device was mounted on a heater and both contact pads were connected *via* a needle probe. A mass flow controlled gas calibration system was used for mixing a high purity (99.999%) dry synthetic air and 1% H_2 gas balanced in synthetic air, at different concentrations, and purging them into the chamber at a constant gas flow of 200 SCCM.

For the current-voltage (*I*-*V*) measurements, a Keithley 2606 source meter was used in order to set the bias voltage and measure the current through the devices. During the testing, the operating temperatures of the devices were altered in the range of 22 to 100 °C. The dynamic response of the sensors was measured as a change in the voltage magnitude, while the sensors were biased at a constant current of 100 μA and exposed to synthetic air with a H_2

balance concentration in the order of 0.06% to 1%. The response and recovery time of the sensors is defined as the time duration needed for the device to undergo a voltage change from 10% to 90% from the no exposure to the fully exposed condition [39]. An Agilent 34410A digital multimeter was utilized to record the voltage changes. A detailed schematic diagram of the measurement set-up can be seen in Figure 2.

3. Results and discussion

3.1 Nb_2O_5 films characterizations

Figure 3 shows the cross-sectional, top, and bottom view SEM images of nanoporous Nb_2O_5 after the anodization and annealing processes (SEM images of porous Nb_2O_5 before annealing can be viewed in Figure S2 of Supplementary). As can be seen in Figure 3(b), a highly organized pore distribution is observed, with nanosized pore opening diameters ranging from 30 to 50 nm. The side walls are around 10 to 20 nm thick. The higher magnification images of cross-sectional view of the nanoporous film in Figure 3(c) show highly packed vein-like nanostructured networks. The nanoveins have internal diameters ranging from 30 to 50 nm with "nanopassage" of diameters as small as 10 nm and there are also occasional lateral interconnections. The bottom of the anodized layer consists of uniform and packed pseudo-semispheres with diameters of approximately 50 nm (Figure 3(d)). As described earlier, Pt was sputtered onto the surface of the Nb_2O_5 to form the catalytic and contact layer. As can be seen in Figure 4(a), the Pt layer was found to nicely conform onto the top of the pore walls. The conformation continues into forming a smooth surface on the top of the photoresist that establishes the extended contact pad, as shown in Figure 4(b). In order to confirm Pt covers inside the nanoporous Nb_2O_5 films, we have characterized the films using energy dispersive X-ray (EDX). We have performed the EDX measurement at 15 different locations for top, middle and bottom part of 1 and 2 μm thick nanoporous Nb_2O_5

films which is presented in Figure 5. The EDX measurements show the presence of Pt in the depth of both nanoporous Nb_2O_5 films.

The XRD results of the as-anodized and annealed nanoporous Nb_2O_5 are shown in Figure S3 in the supporting information. From these patterns, the as-anodized sample shows an amorphous phase with niobium metal peaks at ~39° and ~56° (ICDD 35-0789). Whereas the annealed nanoporous Nb_2O_5 sample obviously shows a dominant orthorhombic phase (ICDD 27-1003, a=6.168, b=29.312 and c=3.936 Å), as distinguished by peaks appearing at 22.6, 28.3, 36.6, 42.4, 46.2, 49.7, 55.1, 58.3 and 63.1° [31]. Furthermore, Raman spectra measurements (Figure S4 in the supporting information) has shown a board peak, centred around 650 cm^{-1}, which represents the symmetric stretching mode of *v* (O-Nb-O) in amorphous niobium oxide [40]. Other weak peaks at 248 and 900 cm^{-1} can be assigned to the terminal Nb=O vibrational bond and bending modes of Nb-O-Nb linkages, respectively. The Raman peaks become more distinguished after annealing with a peak shift from 650 to 690 cm^{-1}, and two new peaks appear at 303 and 460 cm^{-1}, which both indicate the orthorhombic nature of the annealed nanoporous network [31, 41, 42].

An XPS analysis was employed to determine the chemical composition and valences of the nanoporous Nb_2O_5. Figure 6(a) shows the survey spectrum of the annealed Nb_2O_5 film. The signals of Nb and O are visible, confirming the presence of niobium and oxygen elements. As shown in Figure 6(b), the high-resolution spectrum for the Nb region exhibits the $Nb3d_{3/2}$ peak at 210.08 eV and $Nb3d_{5/2}$ at 207.28 eV. The spectra obtained indicate that the film is composed of Nb_2O_5, which is consistent with a previous report [43]. The existence of low peak of C1s in the survey spectrum is expected due to CO_2 adsorption or contamination carbon from the environment. Unlike other metal oxides such as anodized TiO_2 [44], the XPS pattern shows that there is no fluoride doping effect after the anodization process, which is

beneficial for reducing the internal electron scattering during the passage of electrical current in Nb_2O_5 [31].

3.2 Gas sensing

The Pt/Nb/Nb_2O_5/Pt metal-semiconductor-metal (MSM) structure sensing mechanism can be described by the adsorption of the hydrogen molecules, H_2 on the catalytic Pt layer. The hydrogen molecules are then dissociated into hydrogen atoms which transfer through the Pt layer onto the Nb_2O_5 interface [7, 45]. The hydrogen atom diffuses along the interface of the Nb_2O_5 and eventually intercalate with metal oxide. These activities contribute to change of the barrier height, which allows carriers with sufficient energies to flow over the lowered barrier easily *via* the thermionic emission mechanism. Therefore, the junction exhibits a current shift in its *I-V* characteristics upon exposure to the target gas.

Based on the thermionic emission equation [46], the *I-V* relationship of the Pt-Nb_2O_5 junction is given by the following equation:

$$I = I_s exp\left(\frac{qV}{nkT}\right)\left[1 - exp\left(-\frac{qV}{kT}\right)\right], \quad (1)$$

where I_s is the saturation current, q is the electron charge, V is the applied voltage, T is the absolute temperature in Kelvin, n is the ideality factor, and k is Boltzmann's constant. The ideality factor is introduced to take into account the deviation of the experimental *I-V* graph from the ideal thermionic model. In this equation, the saturation current I_s is given by [46]:

$$I_s = AA^{**}T^2 exp\left(-\frac{q\Phi_{b0}}{kT}\right), \quad (2)$$

in which A, A^{**} and Φ_{b0} are the contact area, the Richardson constant and the zero-bias Schottky barrier height (SBH), respectively.

In our work, the behavior of the gas sensor based on nanoporous Nb_2O_5 was first studied under different operating temperatures. These measurements were conducted for the 1 μm film thickness sensor by exposing it to synthetic air and 1% H_2 gas balanced in synthetic air at operating temperatures of 22, 50, 80 and 100 °C. Temperatures above 100 °C could not be implemented as the photoresist protection, forming the extended electrode, deteriorated at such elevated temperatures. At near room temperature, the charge carriers have insufficient energy to overcome the barrier height energy [47]. As a result, the current is relatively low. At elevated temperatures, the energy of the carriers is greater than room temperature thus allowing a larger flow of current. Current increases as the temperature increases further and the difference between the exposed and non-exposed states of the sensor can be clearly observed. From the *I-V* characteristics in Figure 7, it can be seen that the sensor exhibited the largest current shifts after the exposure to H_2 at 100 °C. The device also shows symmetrical *I -V* curves, which is in agreement with the typical electrical properties of a MSM structure [46, 48].

The dynamic responses of the 1 μm sensor towards 0.06, 0.12, 0.25, 0.5, and 1.0% of H_2 gas at operating temperatures of 50 and 100 ºC are presented in Figure 8. The sensor was biased at a constant current of 100 μA and exposed to synthetic air and different concentrations of H_2 gas at 600 s intervals. As can be seen, when the ambient is repeatedly switched from air to H_2 gas, the baseline remains stable. At 100 ºC, the 1 μm sensor produced voltage shifts of 0.468 and 2.179 V towards 0.06% and 1.0% concentrations of H_2 gas, respectively. Whereas at 50 ºC at these H_2 gas concentrations the sensor exhibited voltage shifts of 0.44 and 1.89 V, respectively. The results clearly indicate that the 1 μm sensor demonstrate a higher sensitivity when operate at 100 ºC compared to the operation at 50 ºC. This improvement is generally ascribed to the better catalytic effect of Pt at higher temperatures [49].

In order to assess the effect of thickness on sensor performance, the experiments were further continued for a sensor with a 2 µm film thickness at the operating temperature of 100 ºC. Figure 9 shows dynamic responses of the 1 and 2 µm sensors towards different concentrations of H_2 gas at 100 ºC. For the 1 µm sensor, the response times ($t_{10\%-90\%}$) of 142, 236, 260, 179 and 90 s, and the recovery times ($t_{90\%-10\%}$) of 491, 432, 413, 367, and 331 s were measured towards 0.06, 0.12, 0.25, 0.5, and 1.0% of H_2 gas, respectively. Meanwhile, with the same set of H_2 gas concentrations, the 2 µm sensor produced response times ($t_{10\%-90\%}$) of 189, 166, 226, 123 and 88 s, and recovery times ($t_{90\%-10\%}$) of 515, 411, 434, 288 and 478 s, respectively. The response and recovery times have similar values to that of the Nb_2O_5 nanowire gas sensor reported by Wang *et al.* [24]. Overall, both sensors show a fairly similar trend in terms of response and recovery time, where the response time is much shorter than the recovery time (Figure 10). For the sensing performance comparison, the maximum voltage shift *vs* H_2 gas concentration graphs are presented in Figure 11. The results show that the 1 µm sensor exhibits higher voltage shifts than the 2 µm sensor.

Sakai *et al.* discussed the influence of film thickness on the sensor's response towards H_2 gas by assuming that the gas molecules move inside the nanoporous film with the diffusion coefficient of D_k that can be calculated using the Knudsen equation [50]:

$$D_k = 9700r \times \sqrt{T/M}, \quad (4)$$

where r is the pore radius (cm), T is the temperature (K) and M is the molecular weight of gas (H_2 molecular weight = 2.016 g/mol). The H_2 gas molecule reaction with the metal oxide oxygen atoms along the diffusion path is expressed by the following transport equation at the steady state condition ($\partial C_A/\partial t = 0$ in which t is time) [50]:

$$0 = D_k\left(\frac{\partial^2 C_A}{\partial x^2}\right) - kC_A \cdot \quad (5)$$

Here, C_A is the concentration of the target gas, x is distance from the film surface, and k is the rate constant of the surface reaction. By applying the boundary conditions on Eq. (5), the following equation can be obtained [50]:

$$C_A(x) = C_{A,s}\,\frac{\sinh\left(x\sqrt{k/D_k}\right)+\sinh\left((2L-x)\sqrt{k/D_k}\right)}{\sinh\left(2L\sqrt{k/D_k}\right)}, \quad (6)$$

in which L is the thickness of the porous film, and $C_{A,s}$ is the concentration of H_2 in the surrounding atmosphere (x=0). We used Eqs. (4) and (6) to estimate the dependence of the gas response on our nanoporous Nb_2O_5 film thickness. In these calculations, we assume that the diffusion coefficient is calculated at 373 K and the pores for both 1 and 2 µm films have average diameters 40 nm. The gas concentration profiles for 1 and 2 µm sensors are presented in Figures 12 (a) and (b), respectively. From the figures, it is obvious that the steady state gas diffusions within both layers are similar and at 0.5 µm they reach 0.77 % of the surface gas concentration value. This means that in both 1 and 2 µm thick films almost only the top sections of the layers interact with the gas. As a result, a much larger ration of the 2 µm thick film is not affected by the gas and the relative change in the response of the 2 µm film is less than the 1 µm film.

The mechanism of the nanoporous Nb_2O_5 gas sensing is presented in Figure S5 in the supporting information. In these sensors, H_2 gas molecules are broken down to $2H^+$ by the Pt catalytic layer. After the initial diffusion of H^+ atoms, it is suggested that they intercalate with Nb_2O_5 pore walls [51, 52] that can be described using the following formula:

$$Nb_2O_5 + xH^+ + xe^- \leftrightharpoons H_xNb_2O_5 \quad (7)$$

However, the system is kept at an elevated temperature. As a result, it is also possible that eventually $H_xNb_2O_5$ breaks down, producing reduced niobium oxide and H_2O molecules in a process that similarly occurs during the interaction of H_2 with WO_3 at such a temperature [51]:

$$2H_xNb_2O_5 \leftrightharpoons xH_2O + 2Nb_2O_{5-x/2} \quad (8)$$

When the film is exposed to air (oxygen), the reduced film surface reverts back to its original fully oxidized state, which is described by the following reaction:

$$(x/4)O_2 + Nb_2O_{5-x/2} \leftrightharpoons Nb_2O_5 \quad (9)$$

The released electrons in Eq. (7) reduce the length of the depletion region in the Nb_2O_5 film. They both enhance the conductivity of the film and decrease the barrier height, which correspond to the voltage shift for the gas sensors. When the film is exposed to air (oxygen), the depletion region will be rebuilt by the adsorbed oxygen species and the resistance will increase to its initial level. Thus, the voltage of the gas sensor returns back to its baseline value.

4. Conclusions

We have demonstrated the effectiveness of nanoporous Nb_2O_5 films with nanovein-like networks for H_2 gas sensing. High porosity Nb_2O_5 films were synthesized *via* a highly tuned anodization process at an elevated temperature in a fluoride-organic solvent containing a small percentage of water. The increased surface to volume ratio structure provided by the nanoporous Nb_2O_5 films allow the gas molecules to penetrate and adsorb into the nanoporous films resulting in a high sensitivity sensor which shows a good return to the baseline after recovery. The sensor response was dependent on the Nb_2O_5 film thickness, which was both experimentally and theoretically discussed. The simple and low-cost sensors described here

could be used for sensing gas species other than H_2 and sensing selected chemical components.

Acknowledgements

The authors acknowledge the facilities, and the scientific and technical assistance, of the Australian Microscopy & Microanalysis Research Facility at the RMIT Microscopy & Microanalysis Facility (RMMF), at RMIT University.

References

[1] C. Wang, L. Yin, L. Zhang, D. Xiang, R. Gao, Metal Oxide Gas Sensors: Sensitivity and Influencing Factors, Sensors, 10 (2010) 2088-2106.

[2] G. Eranna, B. C. Joshi, D. P. Runthala, R.P. Gupta, Oxide materials for development of integrated gas sensors - A comprehensive review, Crit. Rev. Solid State 29 (2004) 111-188.

[3] E. Comini, Metal oxide nano-crystals for gas sensing, Anal. Chim. Acta 568 (2006) 28-40.

[4] S. Basu, P.K. Basu, Nanocrystalline metal oxides for methane sensors: Role of noble metals, J. Sens., 2009 (2009) 1-20.

[5] M.A. Andio, P.N. Browning, P.A. Morris, S.A. Akbar, Comparison of gas sensor performance of SnO_2 nano-structures on microhotplate platforms, Sens. Actuators, B 165 (2012) 13-18.

[6] M. Shafiei, K. Kalantar-zadeh, W. Wlodarski, Hydrogen gas sensing performance of Pt/SnO_2 nanowires/SiC MOS devices, International Journal On Smart Sensing And Intelligent Systems, 1 (2008).

[7] J. Yu, S.J. Ippolito, W. Wlodarski, M. Strano, K. Kalantar-zadeh, Nanorod based Schottky contact gas sensors in reversed bias condition, Nanotechnol., 21 (2010) 265502.

[8] Y. Li, X. Yu, Q. Yang, Fabrication of TiO_2 nanotube thin films and their gas sensing properties, J. Sens., 2009 (2009).

[9] S.D. Shinde, G.E. Patil, D.D. Kajale, V.B. Gaikwad, G.H. Jain, Synthesis of ZnO nanorods by spray pyrolysis for H_2S gas sensor, J. Alloys Compd. , 528 (2012) 109-114.

[10] J. Lee, D.H. Kim, S.-H. Hong, J.Y. Jho, A hydrogen gas sensor employing vertically aligned TiO_2 nanotube arrays prepared by template-assisted method, Sens. Actuators, B, 160 (2011) 1494-1498.

[11] J. Kukkola, J. Mäklin, N. Halonen, T. Kyllönen, G. Tóth, M. Szabó, A. Shchukarev, J.-P. Mikkola, H. Jantunen, K. Kordás, Gas sensors based on anodic tungsten oxide, Sens. Actuators, B, 153 (2011) 293-300.

[12] P. Sowti Khiabani, A. Hosseinmardi, E. Marzbanrad, S. Ghashghaie, C. Zamani, M. Keyanpour-Rad, B. Raissi, NO_2 gas sensor fabrication through AC electrophoretic deposition from electrospun In_2O_3 nanoribbons, Sens. Actuators, B, 162 (2012) 102-107.

[13] P. Sun, X. He, W. Wang, J. Ma, Y. Sun, G. Lu, Template-free synthesis of monodisperse alpha-Fe_2O_3 porous ellipsoids and their application to gas sensors, CrystEngComm, 14 (2012) 2229-2234.

[14] K.J. Choi, H.W. Jang, One-dimensional oxide nanostructures as gas-sensing materials: Review and issues, Sensors, 10 (2010) 4083-4099.

[15] H.T. H. Kondo, T. Takeuchi, I. Igarashi, Nb_2O_5 thin-film oxygen sensor, Proc. 3rd Sensor Symp., Japan, (1983) 185-190.

[16] D. Rosenfeld, P.E. Schmid, S. Széles, F. Lévy, V. Demarne, A. Grisel, Electrical transport properties of thin-film metal-oxide-metal Nb_2O_5 oxygen sensors, Sens. Actuators, B, 37 (1996) 83-89.

[17] L. Chambon, C. Maleysson, A. Pauly, J.P. Germain, V. Demarne, A. Grisel, Investigation, for NH_3 gas sensing applications, of the Nb_2O_5 semiconducting oxide in the

presence of interferent species such as oxygen and humidity, Sens. Actuators, B, 45 (1997) 107-114.

[18] L. Chambon, A. Pauly, J.P. Germain, C. Maleysson, V. Demarne, A. Grisel, A model for the responses of Nb_2O_5 sensors to CO and NH_3 gases, Sens. Actuators, B, 43 (1997) 60-64.

[19] L. Chambon, J.P. Germain, A. Pauly, V. Demarne, A. Grisel, A metallic oxide gas sensor array for a selective detection of the CO and NH_3 gases, Sens. Actuators, B, 60 (1999) 138-147.

[20] T. Hyodo, J. Ohoka, Y. Shimizu, M. Egashira, Design of anodically oxidized Nb_2O_5 films as a diode-type H_2 sensing material, Sens. Actuators, B, 117 (2006) 359-366.

[21] U. Cvelbar, K. Ostrikov, A. Drenik, M. Mozetic, Nanowire sensor response to reactive gas environment, Appl. Phys. Lett., 92 (2008) 133505-133503.

[22] T. Hyodo, H. Shibata, Y. Shimizu, M. Egashira, H_2 sensing properties of diode-type gas sensors fabricated with Ti- and/or Nb-based materials, Sens. Actuators, B, 142 (2009) 97-104.

[23] H.G. Moon, H.W. Jang, J.-S. Kim, H.-H. Park, S.-J. Yoon, A route to high sensitivity and rapid response Nb_2O_5-based gas sensors: TiO_2 doping, surface embossing, and voltage optimization, Sens. Actuators, B, 153 (2011) 37-43.

[24] Z. Wang, Y. Hu, W. Wang, X. Zhang, B. Wang, H. Tian, Y. Wang, J. Guan, H. Gu, Fast and highly-sensitive hydrogen sensing of Nb_2O_5 nanowires at room temperature, Int. J. Hydrogen Energy 37 (2012) 4526-4532.

[25] X. Xiao, G. Dong, C. Xu, H. He, H. Qi, Z. Fan, J. Shao, Structure and optical properties of Nb_2O_5 sculptured thin films by glancing angle deposition, Appl. Surf. Sci., 255 (2008) 2192-2195.

[26] A. Le Viet, R. Jose, M.V. Reddy, B.V.R. Chowdari, S. Ramakrishna, Nb_2O_5 photoelectrodes for dye-sensitized solar cells: Choice of the polymorph, J. Phys. Chem. C 114 (2010) 21795-21800.

[27] J.H.L. Jinsub Choi, Jaeyoung Lee and Kyung Ja Kim, Porous niobium oxide films prepared by anodization–annealing–anodization, Nanotechnol., 18 (2007).

[28] M.S. Michel A. Aegerter, and Yeping Guo, Sol-gel niobium pentoxide coatings: Applications to photovoltaic energy conversion and electrochromism, Int. J. Photoenergy, 4 (2002) 1-10.

[29] S.H. Mujawar, A.I. Inamdar, C.A. Betty, V. Ganesan, P.S. Patil, Effect of post annealing treatment on electrochromic properties of spray deposited niobium oxide thin films, Electrochim. Acta, 52 (2007) 4899-4906.

[30] A.L. Viet, M.V. Reddy, R. Jose, B.V.R. Chowdari, S. Ramakrishna, Nanostructured Nb_2O_5 polymorphs by electrospinning for rechargeable lithium batteries, J. Phys. Chem. C 114 (2009) 664-671.

[31] J.Z. Ou, R.A. Rani, M.-H. Ham, M.R. Field, Y. Zhang, H. Zheng, P. Reece, S. Zhuiykov, S. Sriram, M. Bhaskaran, R.B. Kaner, K. Kalantar-zadeh, Elevated temperature anodized Nb_2O_5: A photoanode material with exceptionally large photoconversion efficiencies, ACS Nano, 6 (2012) 4045-4053.

[32] H. Zhang, Y. Wang, D. Yang, Y. Li, H. Liu, P. Liu, B.J. Wood, H. Zhao, Directly hydrothermal growth of single crystal $Nb_3O_7(OH)$ nanorod film for high performance dye-sensitized solar cells, Adv. Mater., 24 (2012) 1598-1603.

[33] H. Habazaki, Y. Oikawa, K. Fushimi, Y. Aoki, K. Shimizu, P. Skeldon, G.E. Thompson, Importance of water content in formation of porous anodic niobium oxide films in hot phosphate-glycerol electrolyte, Electrochim. Acta 54 (2009) 946-951.

[34] M. Habibi, R. Mokhtari, First observation on S-doped Nb_2O_5 nanostructure thin film coated on carbon fiber paper using sol–gel dip-coating: Fabrication, characterization, visible light sensitization, and electrochemical properties, J. Inorg. Organomet. Polym. Mater. , 22 (2012) 158-165.

[35] X. Fang, L. Hu, K. Huo, B. Gao, L. Zhao, M. Liao, P.K. Chu, Y. Bando, D. Golberg, New ultraviolet photodetector based on individual Nb_2O_5 nanobelts, Adv. Funct. Mater. , 21 (2011) 3907-3915.

[36] H. Wen, Z. Liu, J. Wang, Q. Yang, Y. Li, J. Yu, Facile synthesis of Nb_2O_5 nanorod array films and their electrochemical properties, Appl. Surf. Sci., 257 (2011) 10084-10088.

[37] R. Ghosh, M.K. Brennaman, T. Uher, M.-R. Ok, E.T. Samulski, L.E. McNeil, T.J. Meyer, R. Lopez, Nanoforest Nb_2O_5 photoanodes for dye-sensitized solar cells by pulsed laser deposition, ACS Appl. Mater. Interfaces, 3 (2011) 3929-3935.

[38] Z. I, Electrolytic deposition of niobium oxide films, Materials Letters, 35 (1998) 188-193.

[39] J. Huang, Q. Wan, Gas Sensors Based on Semiconducting Metal Oxide One-Dimensional Nanostructures, Sensors, 9 (2009) 9903-9924.

[40] J.M. Jehng, I.E. Wachs, Structural chemistry and Raman spectra of niobium oxides, Chem. Mater. , 3 (1991) 100-107.

[41] B. Orel, M. Maček, J. Grdadolnik, A. Meden, In situ UV-Vis and ex situ IR spectroelectrochemical investigations of amorphous and crystalline electrochromic Nb_2O_5 films in charged/discharged states, Journal of Solid State Electrochemistry, 2 (1998) 221-236.

[42] D. Falcomer, A. Speghini, G. Ibba, S. Enzo, C. Cannas, A. Musinu, M. Bettinelli, Morphology and Luminescence of Nanocrystalline Nb2O5 Doped with Eu3+, Journal of Nanomaterials, 2007 (2007).

[43] S. Ge, H. Jia, H. Zhao, Z. Zheng, L. Zhang, First observation of visible light photocatalytic activity of carbon modified Nb_2O_5 nanostructures, J. Mater. Chem. , 20 (2010) 3052-3058.

[44] D. Regonini, A. Jaroenworaluck, R. Stevens, C.R. Bowen, Effect of heat treatment on the properties and structure of TiO_2 nanotubes: Phase composition and chemical composition, Surf. Interface Anal. , 42 (2010) 139-144.

[45] K. Skucha, Z.Y. Fan, K. Jeon, A. Javey, B. Boser, Palladium/silicon nanowire Schottky barrier-based hydrogen sensors, Sens. Actuators, B 145 (2010) 232-238.

[46] S.M. Sze, K.K. Ng, Physics of semiconductor devices, 3rd ed., Wiley, 2007.

[47] M. Shafiei, P.G. Spizzirri, R. Arsat, J. Yu, J. du Plessis, S. Dubin, R.B. Kaner, K. Kalantar-zadeh, W. Wlodarski, Platinum/Graphene nanosheet/SiC contacts and their application for hydrogen gas sensing, J. Phys. Chem. C, 114 (2010) 13796-13801.

[48] S.-Y. Chiu, H.-W. Huang, T.-H. Huang, K.-C. Liang, K.-P. Liu, J.-H. Tsai, W.-S. Lour, Comprehensive study of Pd/GaN metal–semiconductor–metal hydrogen sensors with symmetrically bi-directional sensing performance, Sensors and Actuators B: Chemical, 138 (2009) 422-427.

[49] S. Junghui, L. Wu, Operation of Pt/AlGaN/GaN-Heterojunction Field-Effect-Transistor Hydrogen Sensors With Low Detection Limit and High Sensitivity, Electron Device Letters, IEEE, 29 (2008) 1193-1195.

[50] G. Sakai, N.S. Baik, N. Miura, N. Yamazoe, Gas sensing properties of tin oxide thin films fabricated from hydrothermally treated nanoparticles: Dependence of CO and H_2 response on film thickness, Sens. Actuators, B 77 (2001) 116-121.

[51] M.H. Yaacob, M. Breedon, K. Kalantar-zadeh, W. Wlodarski, Absorption spectral response of nanotextured WO_3 thin films with Pt catalyst towards H_2, Sens. Actuators, B, 137 (2009) 115-120.

[52] X. Sha, L. Chen, A.C. Cooper, G.P. Pez, H. Cheng, Hydrogen absorption and diffusion in bulk α-MoO_3, J. Phys. Chem. C 113 (2009) 11399-11407.

435

Author Biographies

Rozina Abdul Rani received her Bachelor of Engineering (Electrical and Electronic) with Honours (2001) and M.Sc. (2007) degrees from Universiti Sains Malaysia, Malaysia. She is currently undertaking her candidature for a Ph.D. at RMIT University. Her research interests include synthesis and characterization of nanostructured metal oxides, dye-sensitized solar cells and chemical sensors.

Ahmad Sabirin Zoolfakar received his Bachelor of Engineering (Electrical) with Honours from Universiti Malaya, Malaysia (2001) and Master of Science (Engineering) (Microelectronic Systems and Telecommunications) from The University of Liverpool, UK (2003). He is currently undertaking his PhD at RMIT University, Australia studying p-n heterojunction solar cells and memristor. His research interests include aqueous chemical synthesis, gas vapour synthesis, nanotechnology and materials science.

Jian Zhen Ou received his Bachelor of Engineering (Honours First Class) from RMIT University, Australia in 2008. He is currently at the final stage of his PhD study in RMIT University. His research interests include synthesis and characterization of nanostructured metal oxides, as well as the developments of metal oxides based high performance chemical sensors, smart windows and dye-sensitized solar cells.

Matthew Field received his Doctorate in Applied Physics from RMIT University (Australia) in 2011 and is currently a postdoctoral researcher at RMIT University. His research interests include synthesis of metal oxide thin film coatings for high performance electronic applications, plasma deposition of advanced functional coatings and characterization of such

coatings using a combination of electron microscopy, spectroscopy and synchrotron techniques.

Michael W. Austin received his PhD degree in electronic engineering from the University of London, London, U.K., in 1982. Since then he has been a member of academic staff, and a Professor since 1996, in what is now known as the School of Electrical and Computer Engineering at RMIT University, Melbourne, Australia. He was the Director of RMIT's *Microelectronics and Materials Technology Centre* from 1994 to 2012 and is currently leader of the Functional Materials for Advanced Devices project in RMIT's *Platform Technologies Research Institute.* Professor Austin has over 30 years' experience in micro/nano fabrication technologies and their application in device fabrication.

Kourosh Kalantar-zadeh is an Associate Professor at RMIT University, Australia. He received his B.Sc. (1993) and M.Sc. (1997) degrees from Sharif University of Technology, Iran, and Tehran University, Iran, respectively, and a Ph.D. at RMIT University, Australia (2001). His research interests include chemical and biochemical sensors, nanotechnology, microsystems, materials sciences, electronic circuits, and microfluidics. He is the author of over 200 scientific manuscripts.

Figure Captions

Figure 1: Schematic of: (a) the device's cross-section shows the contact surface extended to enable connection of the contact pad body to the sensing area of Nb_2O_5 coated with Pt and (b) the gas sensor 3D configuration.

Figure 2: Schematic diagram of the measurement set-up.

Figure 3: SEM images of the Nb_2O_5 nanoporous film after the annealing process: (a) cross-sectional view of the whole nanoporous structure, (b) top view of the nanoporous structure, (c) higher magnification SEM images of cross-sectional view of the nanoporous structure, and (d) bottom view of the nanoporous structure.

Figure 4: SEM images of the surface of nanoporous Nb_2O_5: (a) after being coated with the Pt layer. (b) SEM image showing the connection of the Pt layer on the surface of nanoporous Nb_2O_5 and the extended contact pad.

Figure 5: EDX measurements for the Pt coverage (*wt*%) at the top, middle and bottom of the nanoporous Nb_2O_5.

Figure 6. (a) The XPS survey scan of the nanoporous Nb_2O_5 film after annealing in air for 30 min at 440 ºC. (b) The XPS spectrum of Nb 3d peaks of the nanoporous Nb_2O_5 film.

Figure 7: *I-V* characteristics of the 1 μm nanoporous Nb_2O_5 gas sensor measured in synthetic air and 1.0% H_2 gas at temperatures ranging from 22 ºC to 100 ºC.

Figure 8: Dynamic response of the 1 μm nanoporous Nb_2O_5 gas sensor measured towards different concentrations of H_2 gas at 50 ºC and 100 ºC at a constant bias current of 100 μA.

Figure 9: Dynamic response of 1 and 2 μm nanoporous Nb_2O_5 gas sensors measured with different concentrations of H_2 gas at 100 ºC at a constant bias current of 100 μA.

Figure 10: Comparison of the response transients of 1 and 2 μm nanoporous Nb_2O_5 gas sensors for a concentration of 1.0% H_2 gas at 100 ºC.

Figure 11: Voltage shifts of 1 and 2 μm nanoporous Nb_2O_5 gas sensors at different concentrations of H_2 gas, operating at 100 ºC.

Figure 12: Comparison of the gas concentration profiles inside (a) 1 and (b) 2 μm nanoporous Nb_2O_5 films at a fixed temperature of 373 K.

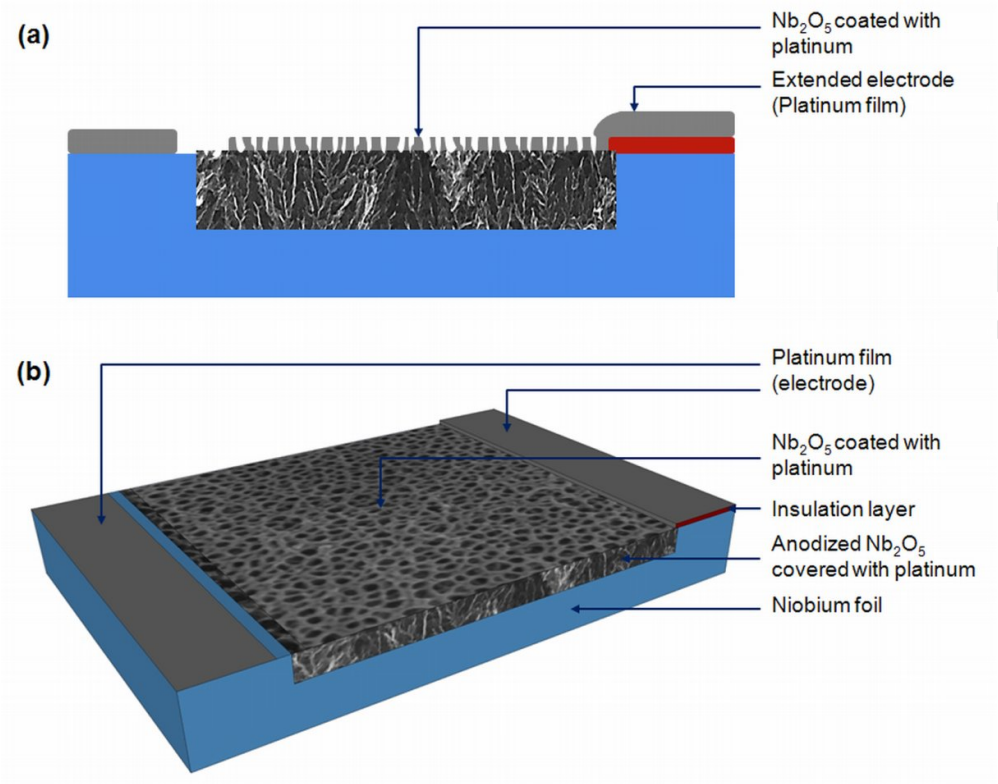

515

Figure 1. Schematic of: (a) the device's cross-section shows the contact surface extended to enable connection of the contact pad body to the sensing area of Nb_2O_5 coated with Pt and (b) the gas sensor 3D configuration.

520

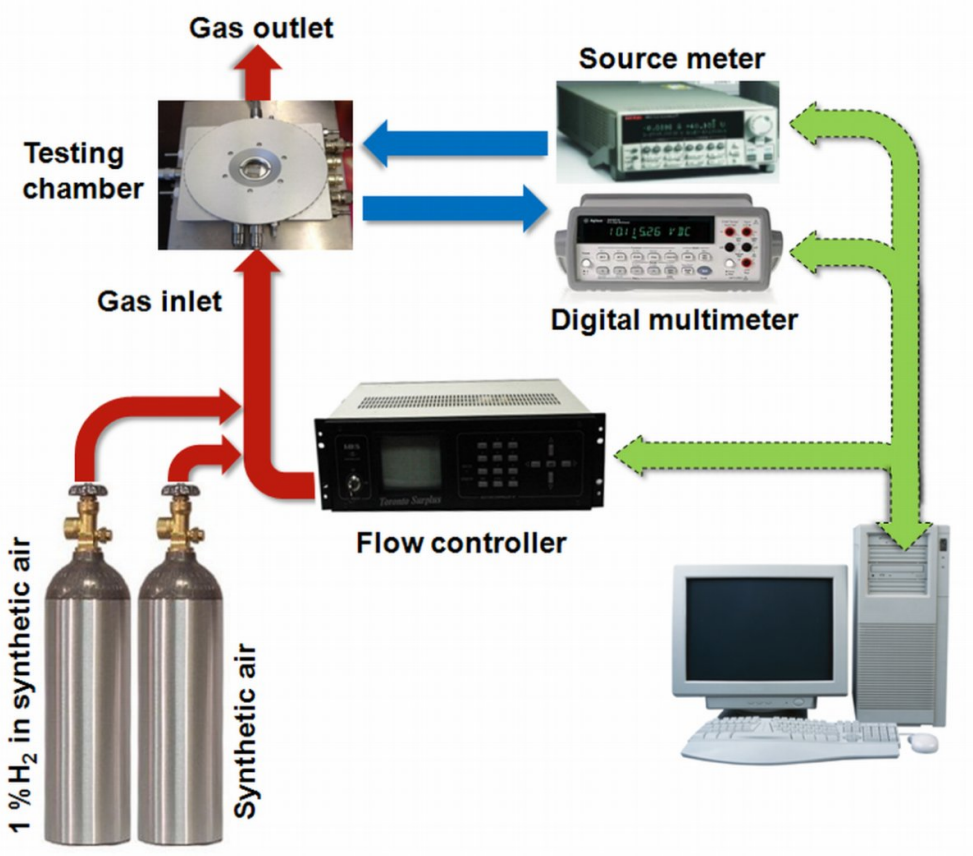

Figure 2. Schematic diagram of the measurement set-up.

525

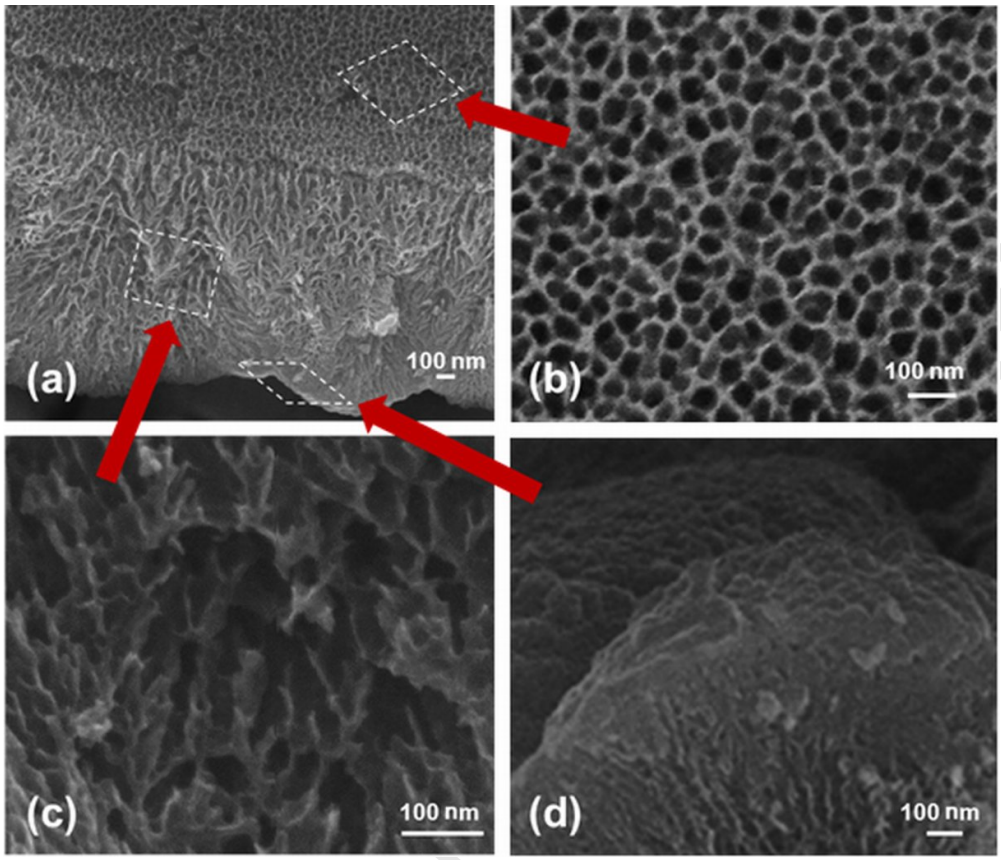

Figure 3. SEM images of the Nb_2O_5 nanoporous film after the annealing process: (a) cross-sectional view of the whole nanoporous structure, (b) top view of the nanoporous structure, (c) higher magnification SEM images of cross-sectional view of the nanoporous structure, and (d) bottom view of the nanoporous structure.

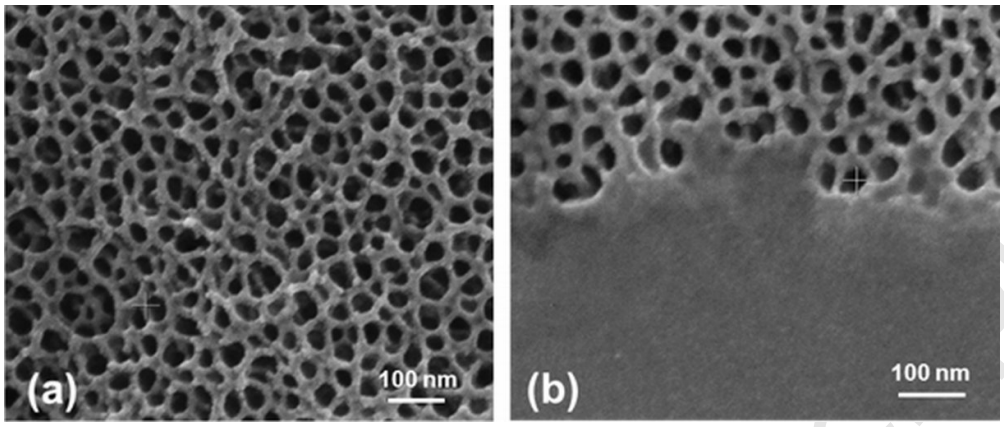

Figure 4. SEM images of the surface of nanoporous Nb_2O_5: (a) after being coated with the Pt layer. (b) SEM image showing the connection of the Pt layer on the surface of nanoporous Nb_2O_5 and the extended contact pad.

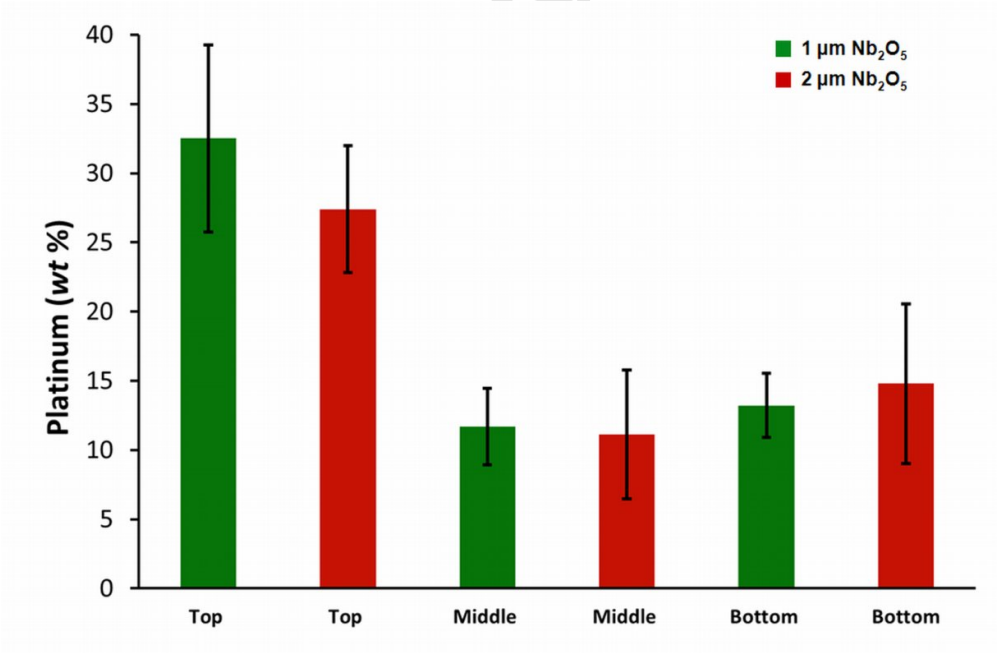

Figure 5. EDX measurements for the Pt coverage (*wt*%) at the top, middle and bottom of the nanoporous Nb_2O_5.

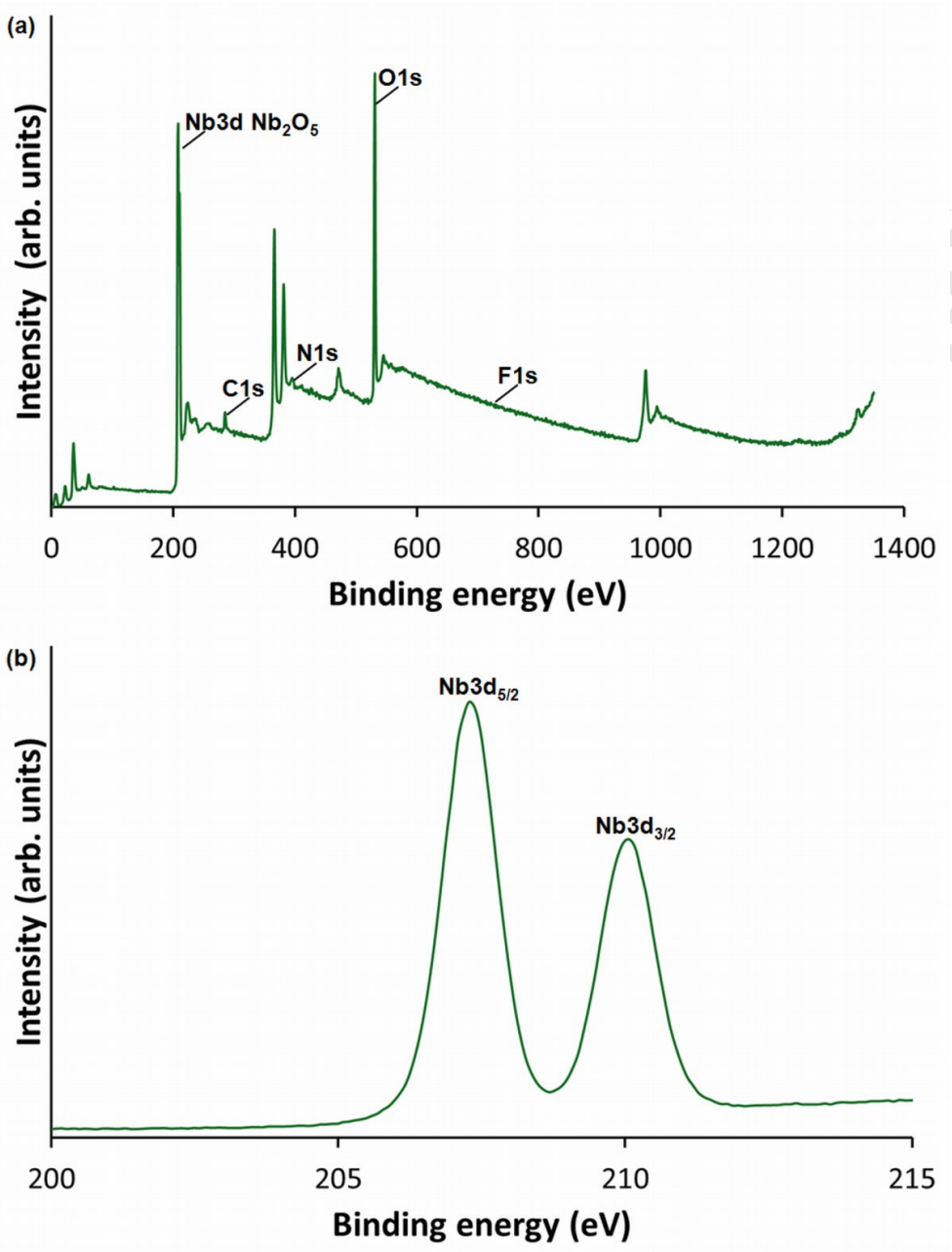

Figure 6. (a) The XPS survey scan of the nanoporous Nb_2O_5 film after annealing in air for 30 min at 440 ºC. (b) The XPS spectrum of Nb 3d peaks of the nanoporous Nb_2O_5 film.

550

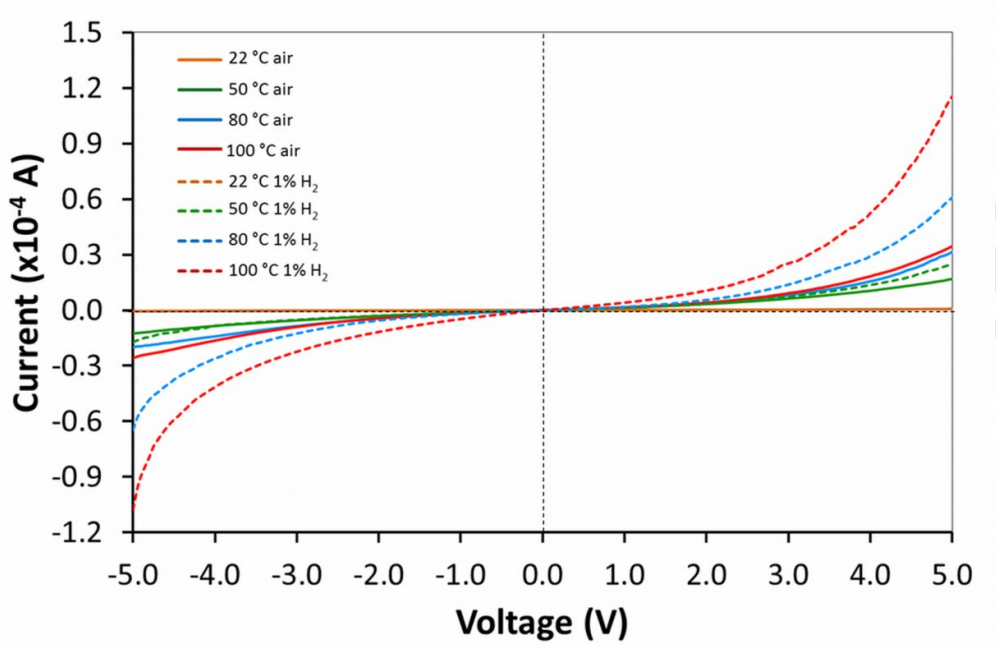

Figure 7. *I-V* characteristics of the 1 μm nanoporous Nb_2O_5 gas sensor measured in synthetic air and 1.0% H_2 gas at temperatures ranging from 22 ºC to 100 ºC.

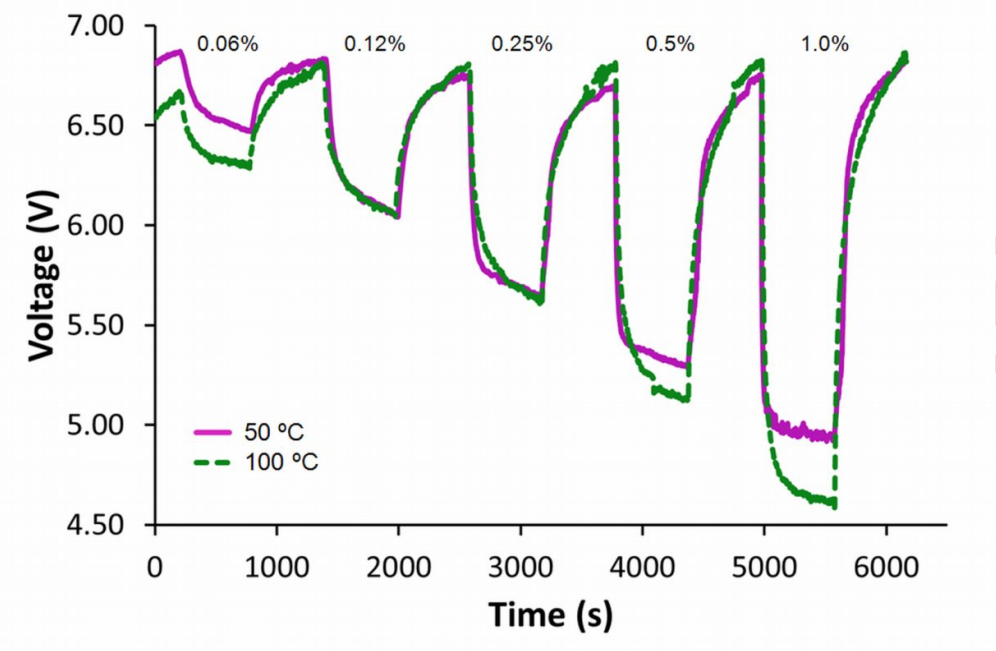

560 Figure 8. Dynamic response of the 1 μm nanoporous Nb_2O_5 gas sensor measured towards different concentrations of H_2 gas at 50 ºC and 100 ºC at a constant bias current of 100 μA.

565

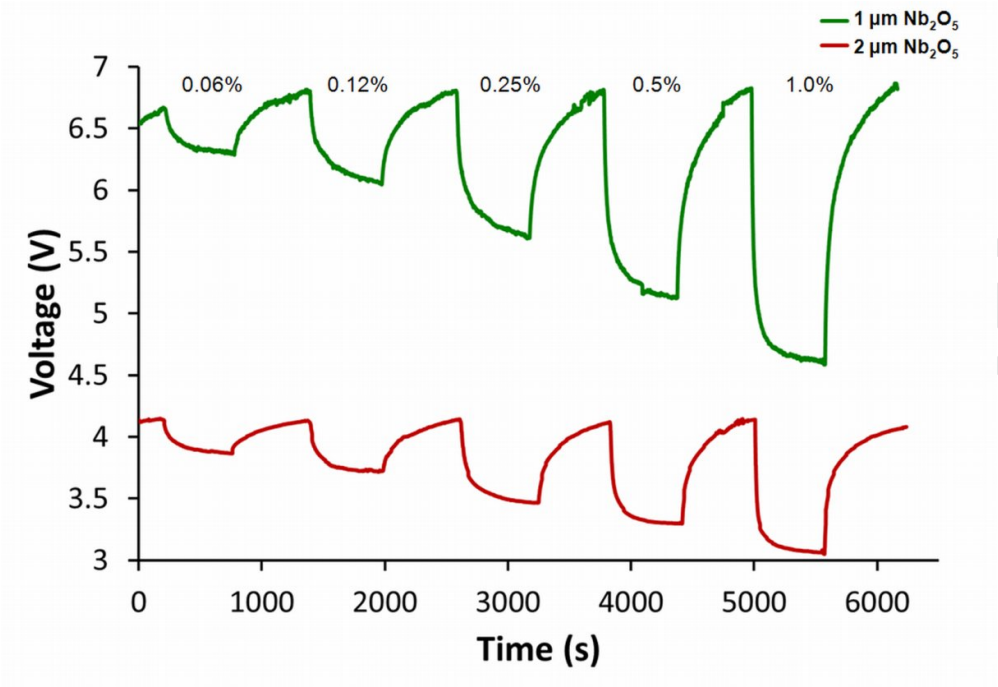

Figure 9. Dynamic response of 1 and 2 µm nanoporous Nb_2O_5 gas sensors measured with different concentrations of H_2 gas at 100 ºC at a constant bias current of 100 µA.

570

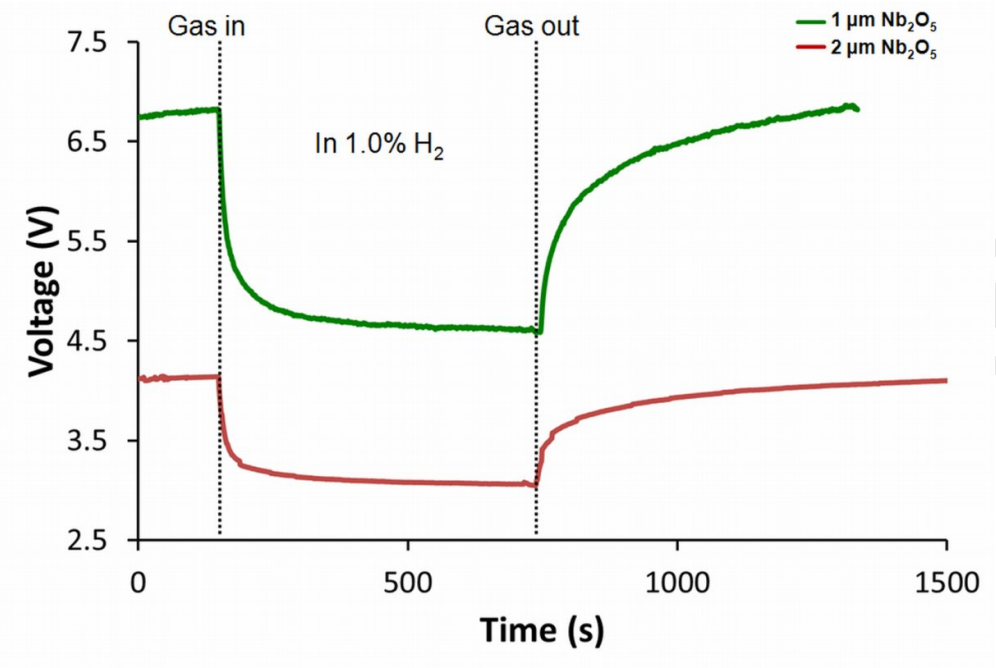

Figure 10. Comparison of the response transients of 1 and 2 µm nanoporous Nb_2O_5 gas sensors for a concentration of 1.0% H_2 gas at100 ºC.

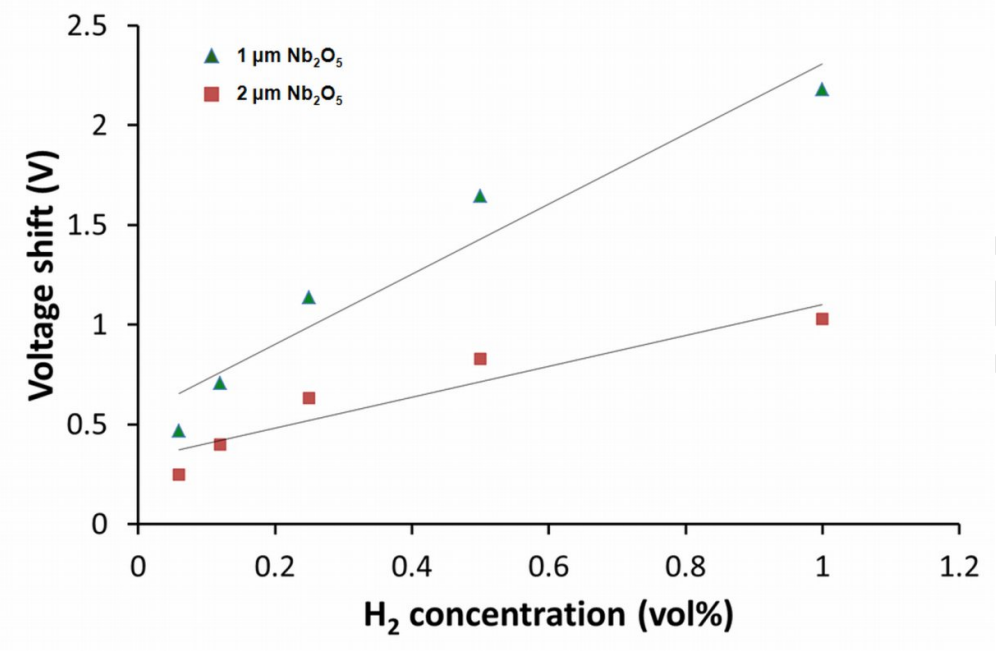

Figure 11. Voltage shifts of 1 and 2 µm nanoporous Nb_2O_5 gas sensors at different concentrations of H_2 gas, operating at 100 ºC.

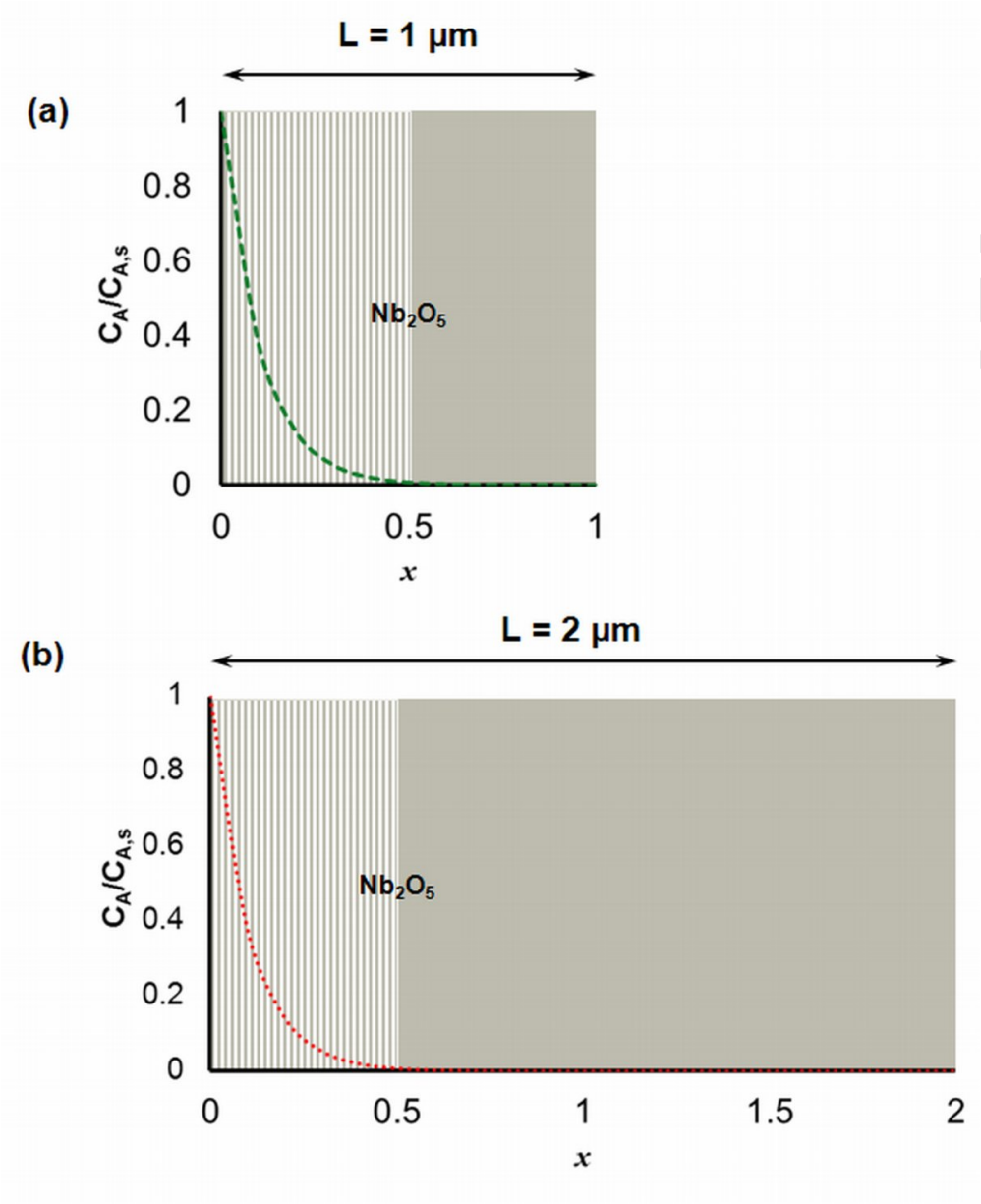

585 Figure 12. Comparison of the gas concentration profiles inside (a) 1 and (b) 2 μm nanoporous Nb_2O_5 films at a fixed temperature of 373 K.